

# Optimization of the soliton self-frequency shift in a tapered photonic crystal fiber

A. C. Judge,<sup>1,\*</sup> O. Bang,<sup>2</sup> B. J. Eggleton,<sup>1</sup> B. T. Kuhlmeier,<sup>1</sup> E. C. Mägi,<sup>1</sup> R. Pant,<sup>1</sup> and C. Martijn de Sterke<sup>1</sup>

<sup>1</sup>Centre for Ultrahigh-Bandwidth Devices for Optical Systems, Institute of Photonics and Optical Sciences, School of Physics, University of Sydney, Sydney, New South Wales 2006, Australia

<sup>2</sup>DTU Fotonik, Department of Photonics Engineering, Technical University of Denmark, Building 345 V, DK-2800 Kongens Lyngby, Denmark

\*Corresponding author: a.judge@physics.usyd.edu.au

Received July 9, 2009; revised September 8, 2009; accepted September 8, 2009;  
posted September 10, 2009 (Doc. ID 113933); published October 16, 2009

Soliton propagation is modeled in a tapered photonic crystal fiber for various taper profiles with the purpose of optimizing the soliton self-frequency shift (SSFS) in such geometries. An optimal degree of tapering is found to exist for tapers with an axially uniform waist. In the case of axially nonuniform waists, an additional enhancement of the SSFS is achieved by varying the taper waist diameter along its length in a carefully designed fashion in order to present an optimal level of group-velocity dispersion to the soliton at each point, thus avoiding the spectral recoil due to the emission of dispersive waves. In doing so, the increased nonlinearity and dispersion engineering afforded by the reduction of the core size are exploited while circumventing the limitation imposed on the soliton redshift by the associated shortening of the red zero-dispersion wavelength.

© 2009 Optical Society of America  
OCIS codes: 060.4370, 060.5530.

## 1. INTRODUCTION

The soliton self-frequency shift (SSFS) is the phenomenon whereby the central frequency of a solitary optical pulse undergoes a redshift while propagating in an optical fiber because of the inelastic, nonlinear scattering of its photons off the molecular lattice of the glass. Since its discovery [1], the SSFS has been exploited as a means of obtaining a source of short, wavelength-tunable pulses [2,3]. Owing to the inherent nonlinearity of the process, the rate of the SSFS is enhanced by increasing the energy density of the pulse. Thus, in order to maximize the light confinement, many of the demonstrations of the SSFS in the past decade have involved guiding structures with transverse dimensions on the scale of a few micrometers, realized either as the core of an index guiding photonic crystal fiber or through the tapering of otherwise weakly nonlinear fibers [4]. Of course, one may also taper already highly nonlinear photonic crystal fiber both to increase further the transverse confinement of the light and to engineer the dispersion toward a particular purpose [5]. Indeed, tapering is useful in this latter respect and has been used as a means of obtaining anomalous dispersion, a requirement for the existence of bright solitons [6], over a wavelength range where a fiber would otherwise be normally dispersive [7]. Thus, longitudinal confinement of the light may be maintained through the balancing of (anomalously) dispersive pulse broadening by the nonlinear phase shift resulting from the Kerr effect. The tapers utilized in this way typically consist of a waist of uniform diameter connected to the untapered fiber by a transition region at both ends [7,8].

The spectral regions of anomalous dispersion are bounded by two zero-dispersion wavelengths (ZDWs) on

the short (first) and long (second) wavelength sides. When the SSFS leads to a soliton's reaching the second ZDW, a cancellation of its redshift occurs, along with strong, resonant emission of low-amplitude waves (dispersive waves, DWs) in the normally dispersive region at longer wavelengths [9,10]. Thus, in effect, the position of the second ZDW marks the upper limit of the spectral region over which the soliton may redshift. This fact has been exploited as a means for limiting the final wavelength of a redshifting pulse at a fixed value independent of the input power [11]. The tapering of a fiber can lead to a shift of the ZDWs to shorter wavelengths, and so, while enhancing the SSFS rate through tighter confinement of the light, tapering may also retard this process by reducing the maximum redshift obtainable. With wide tunability being one of the most attractive aspects of sources exploiting the SSFS, any limit placed on the range of attainable wavelengths detracts from the effectiveness of such a source. Ideally, one would like to take advantage of the reduced fiber lengths required for a given redshift afforded by the increased shift rate in a tapered fiber, while avoiding the compromise implied by the shorter second ZDW. We show that, in a taper with a uniform waist diameter, an optimal degree of tapering exists beyond which the advantages of further increasing the nonlinearity are no longer realized owing to the behavior of the fiber dispersion.

Tapers with an axially nonuniform waist have recently been proposed for the enhancement of several nonlinear processes; in particular, the trapping and blueshift of DWs by a soliton [12] and the generation of a coherent broadband continuum in the mid-infrared [13]. Both of these proposals employ the SSFS along with the longitu-

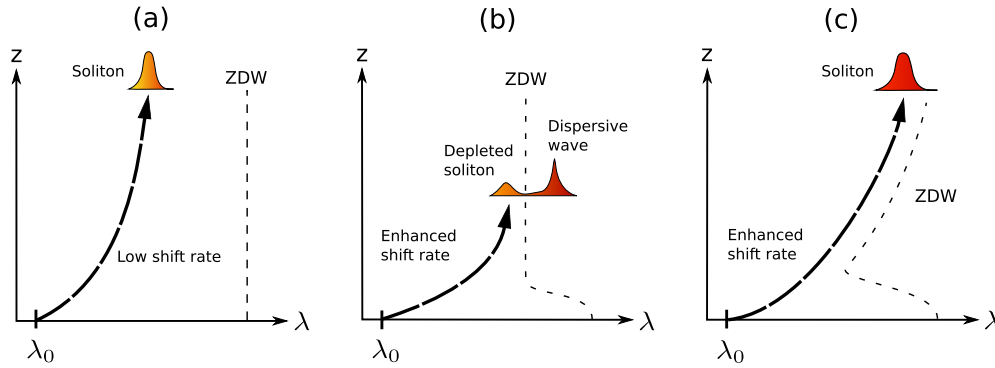


Fig. 1. (Color online) Schematic illustration of the effects of tapering on the SSFS. (a) In the untapered fiber the relatively low nonlinearity and high dispersion lead to a low rate of redshift. (b) Tapering the fiber to a uniform waist enhances the shift rate through a higher nonlinearity but is accompanied by a shortening of the second ZDW. The soliton reaches a point where the dispersion in the taper facilitates the emission of low-amplitude waves in the normally dispersive region with a resultant halt of the redshift. (c) If the waist diameter of the taper is varied such that the soliton experiences the maximum possible nonlinearity and a level of dispersion that minimizes the loss of energy to DWs, the soliton may achieve a redshift above that realized in cases (a) and (b).

dinally varying dispersion of the tapered fiber as key ingredients. Here we investigate a method of designing an optimal taper waist diameter profile that enhances the SSFS rate while mitigating the limitation imposed by the second ZDW. In Fig. 1 we illustrate schematically how this enhancement is achieved. The shift rate in the uniformly tapered fiber [Fig. 1(b)] is higher than that in the untapered fiber [Fig. 1(a)] mainly because of the increased nonlinearity, but the redshift and energy ultimately achieved by the soliton in the taper is compromised by the shorter second ZDW in the waist. In the taper [Fig. 1(c)] with the variable diameter waist the shift rate is enhanced as in the uniform waist taper [Fig. 1(b)], but the progressive increase of the second ZDW at a carefully determined rate removes the associated limitation on the redshift attainable while simultaneously maintaining the group-velocity dispersion (GVD) at the soliton frequency at a level which maximizes the longitudinal confinement of the light but minimizes the emission of DWs.

In exploring the effects of the tapering we consider a single soliton in an idealized scenario in that it possesses a specific initial energy and carrier frequency. In practice, a pulse undergoing SSFS may be obtained from the fission of a larger input pulse [14]. Solitary waves resulting from such a process may manifest with extremely narrow pulse widths  $\leq 10$  fs. We assume in what follows that our soliton is of this origin and that it is sufficiently well isolated both temporally and spectrally that it may be considered independently. After reviewing the basic theory of the SSFS in Section 2, we show in Section 3, through a series of simulations, that an optimal diameter scaling exists for a uniform waist taper, and then we explore how progressively broadening the waist diameter of the taper at the appropriate rate can lead to an increased redshift over that obtained with a standard taper profile.

## 2. THEORY OF THE SSFS

Nonlinear pulse propagation in a single-mode, nonuniform optical fiber in the absence of loss may be modeled by using the generalized nonlinear Schrödinger equation (generalized NSE) [15],

$$\partial_z A(z, T) = i \sum_{m \geq 2} \frac{i^m \beta_m(z) \partial_T^m}{m!} A(z, T) + i \sum_{m \geq 0} \frac{i^m \gamma_m(z) \partial_T^m}{m!} A(z, T) \times \int G(T - T') |A(z, T')|^2 dT'. \quad (1)$$

The pulse amplitude is scaled such that  $|A|^2$  represents the averaged  $z$ -directed pulse power in Watts at delay  $T$  and location  $z$  along the fiber. This leads to the nonlinear parameter taking the form

$$\gamma(z, \omega) = \frac{\omega n(\omega) n_2(\omega)}{c n_{\text{eff}}^2(z, \omega) A_{\text{eff}}(z, \omega)}, \quad (2)$$

where  $n$  is the material refractive index,  $n_2$  is the material nonlinear index,  $n_{\text{eff}}$  and  $A_{\text{eff}}$  are the effective index and area of the fiber mode, respectively, and  $c$  is the vacuum speed of light. The nonlinear response function, of dimension inverse time, is of the form

$$G(T) = \delta(T) + \frac{2f_R}{3(1-f_R)} g_R(T), \quad (3)$$

with  $f_R < 1$  determining the relative magnitude of the delayed nuclear response to the instantaneous electronic contribution. The former is included through  $g_R$ , which has its integral over all time equal to unity. This function is related to the Raman gain as  $\alpha_R = 2 \text{Im}(\tilde{g}_R)$ , where the tilde denotes a Fourier transform. The slightly unconventional form in Eq. (3) is used for convenience, since the real part of the nuclear response may not be considered instantaneous for the short pulse widths considered here; in other words, the nuclear response does not contribute to the nonlinearity associated with the ideal soliton solutions. Thus, the value of  $n_2$  used in Eq. (2) pertains only to the nonlinearity of electronic origin. Finally, the terms  $\beta_m$  and  $\gamma_m$  in Eq. (1) represent the  $m$ th derivative with respect to  $\omega$  of  $\beta$  and  $\gamma$ , respectively, evaluated at the reference frequency  $\omega_0$ .

A distilled form of the generalized NSE, including only the first terms in the summations in Eq. (1) with  $f_R = 0$ , is the NSE,

$$\partial_z A(z, T) = -i \frac{\beta_2 \partial_T^2}{2} A(z, T) + i \gamma_0 A(z, T) |A(z, T)|^2, \quad (4)$$

which, if  $\beta_2 < 0$ , includes the fundamental soliton among its solutions,

$$A(z, T) = \left( \frac{|\beta_2|}{T_s^2 \gamma_0} \right)^{1/2} \operatorname{sech} \left( \frac{T}{T_s} \right) \exp \left( i \frac{|\beta_2|}{2T_s^2} z \right), \quad (5)$$

where  $T_s$  is the characteristic pulse width. As a result of the form of Eq. (3), the form of Eq. (5) with a varying center wavelength remains an approximate solution to Eq. (1) when  $f_R \neq 0$ , for the femtosecond pulse widths considered here. If the more conventional form of the response is used, the soliton solution requires rescaling. If we assume that the energy  $E$  of the soliton is given, along with  $|\beta_2|$  and  $\gamma_0$ , we may express the pulse width as

$$T_s = \frac{2|\beta_2|}{\gamma_0 E}. \quad (6)$$

The theory of the SSFS based upon the NSE with  $f_R \neq 0$  and the assumption of an ideal, fundamental soliton [16] shows the evolution of the center frequency  $\bar{\omega}$  to proceed according to

$$\frac{d\bar{\omega}}{dz} = - \frac{|\beta_2(\bar{\omega})|}{T_s^3(\bar{\omega})} R(\bar{\omega}), \quad (7)$$

where

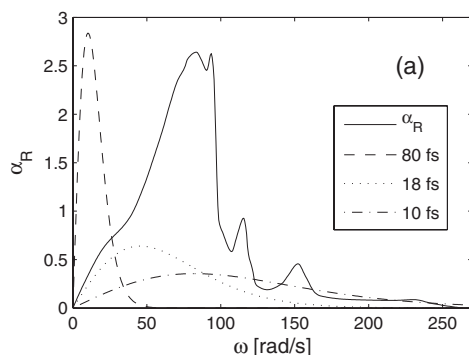
$$\bar{\omega} = \frac{\int \omega |\tilde{A}(\omega)|^2 d\omega}{\int |\tilde{A}(\omega)|^2 d\omega}. \quad (8)$$

The function  $R$  is defined through

$$R = \int \alpha_R(\omega) \mathcal{C}(\omega) \frac{d\omega}{2\pi}, \quad (9)$$

where

$$\mathcal{C}(\omega) = \frac{f_R}{1-f_R} \frac{\pi^2 T_s^4}{6} \frac{\omega^3}{\sinh^2(\pi T_s \omega/2)} \quad (10)$$



is the *convolution function*, so called because it arises from convolution integrals involving the pulse spectrum. The area under each half of this antisymmetric curve, given by the expression  $\int_0^\infty \mathcal{C}(\omega) d\omega / (2\pi)$ , is a constant and is independent of the pulse width. Both  $R$  and the (dimensionless) Raman gain spectrum for silica are displayed in Fig. 2, with the latter overlaid with three examples of the function  $\mathcal{C}$  for different values of  $T_s$ . Two approximations to  $R$  discussed below are also shown. Our definitions differ slightly from those in [16] in order that  $R$  also be dimensionless, and the Raman gain spectrum is obtained from [17].

For pulses of duration  $\geq 80$  fs the gain spectrum is approximately linear in the region where  $\mathcal{C}$  is nonzero and may be approximated by

$$\alpha_R(\omega) \approx \partial_\omega \alpha_R|_{\omega=0}, \quad (11)$$

and  $R$  becomes

$$R \approx R_l = \frac{f_R}{1-f_R} \frac{\Gamma(5)\zeta(4)}{3\pi^4 T_s^4}, \quad (12)$$

where  $\Gamma$  and  $\zeta$  represent the usual special functions. It is from this approximation that the familiar  $1/T_s^4$  dependence of the shift rate arises [16]. The maximum overlap between the gain and convolution functions occurs for  $T_s \sim 18$  fs, and for shorter pulses this is reduced. If the condition  $T_s \ll 2/(\pi \Delta\omega_R)$  is satisfied, where  $\Delta\omega_R$  is the characteristic width of the Raman gain spectrum, we may write

$$\mathcal{C}(\omega) \approx \frac{f_R}{1-f_R} \frac{2T_s^2 \omega}{3}, \quad (13)$$

which leads to

$$R \approx R_s = \frac{f_R}{1-f_R} \frac{2T_s^2}{3} \int \alpha_R(\omega) \omega \frac{d\omega}{2\pi}. \quad (14)$$

In this case the shift rate is proportional to  $T_s^{-1}$  [18]. Also, according to this simplified theory, the rate of the SSFS approaches a finite value at the ZDWs despite the fact that  $T_s \rightarrow 0$ . Of course, in the vicinity of such points the role of higher-order dispersion becomes important, and the assumption of an ideal soliton is inappropriate.

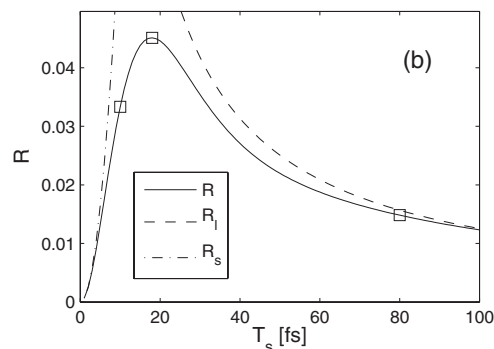


Fig. 2. (a) Raman gain spectrum  $\alpha_R$  for bulk silica overlaid with the convolution function  $\mathcal{C}$  for three values of  $T_s$ . The areas under the latter curves are equal. As indicated, the vertical axis scale corresponds to the dimensionless units of the gain spectrum. The curves drawn with broken lines, referring to the convolution function, have been scaled to convenient but arbitrary units. (b) The functions  $R$ ,  $R_s$ , and  $R_l$ ; the values of  $R$  at the example pulse widths used in panel (a) are indicated with squares.

The dependence of  $R$  on  $\bar{\omega}$  in Eq. (7) arises through allowing the central frequency of the soliton to vary in Eq. (6) to obtain

$$T_s(\bar{\omega}) = \frac{2|\beta_2(\bar{\omega})|}{\gamma(\bar{\omega})E(\bar{\omega})}, \quad (15)$$

which is then inserted into Eq. (10). Changes to the pulse energy in a uniform fiber as a result of the frequency dependence of  $\gamma$  may be included, following Voronin and Zheltikov [19], through

$$E(\bar{\omega}) \approx \frac{E_0 \gamma(\bar{\omega})}{\gamma_0}, \quad (16)$$

where  $E_0$  is the pulse energy at  $\bar{\omega} = \omega_0$ . This is an expression of the conservation law derived from Eq. (1) with  $z$  independent parameters,

$$\partial_z \int \frac{|\tilde{A}(z, \omega)|^2 d\omega}{\gamma(\omega)} = 0, \quad (17)$$

which allows for energy loss due to the dissipative nature of the causal nuclear response. In a nonuniform fiber Eq. (17) is replaced by

$$\partial_z \int \frac{|\tilde{A}(z, \omega)|^2 d\omega}{\gamma(z, \omega)} + \int \frac{|\tilde{A}(z, \omega)|^2}{\gamma(z, \omega)} \partial_z \ln(\gamma(z, \omega)) = 0, \quad (18)$$

which follows directly from Eq. (1). The presence of the second term on the right-hand side ensures that there is no change in the pulse energy due to the nonuniformity of the fiber. From Eq. (18) we may obtain, for an ideal soliton, the approximation

$$E(\bar{\omega}) \approx \frac{E_0 \gamma(z_0, \bar{\omega})}{\gamma_0(z_0)}. \quad (19)$$

Thus the pulse energy is dependent only on the nonlinear coefficient of the initial fiber at  $z = z_0$  and is independent of variations in the fiber, except indirectly through the behavior of  $\bar{\omega}$ .

As an example we use the NL-15-670 fiber from Crystal Fibre. The properties of its fundamental mode are calculated from the SEM image provided on the manufacturer's Website [20] by using the COMSOL package. In Fig. 3 we show the effect of uniformly tapering this example fiber on the values of  $\beta_2$  and  $\gamma$ , as well as the SSFS rate for a soliton of fixed initial energy and carrier frequency, assuming that the tapering process corresponds to a simple scaling of the fiber diameter. It is observed that a reduced core size always leads to an increased SSFS rate over the range of wavelengths considered. By noting the crossings of the various dispersion curves, however, this is not an obvious result, and follows from the explicit form of Eq. (7). In other words, for the case considered here, the increased lateral confinement resulting from the tapering of the fiber plays the dominant role in determining the effect of this process on the rate of redshift of the soliton, and this rate therefore generally decreases with increasing wavelength. However, close to the second ZDW, the adiabatic temporal compression of the soliton due to the decreasing absolute GVD may override the effect of the non-

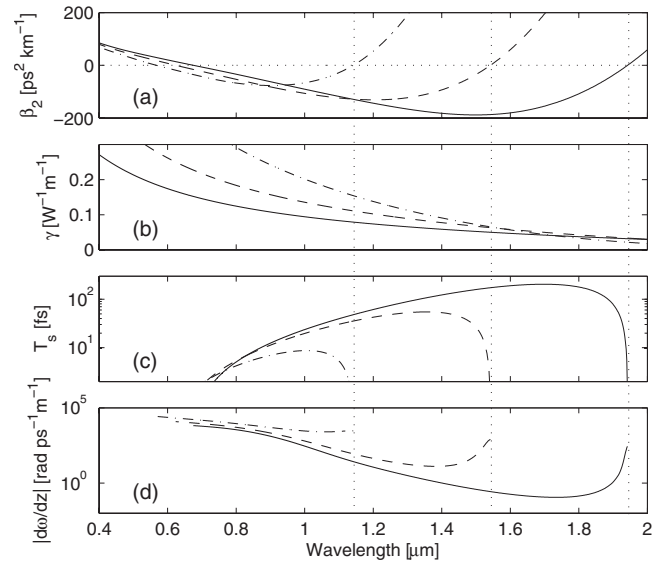


Fig. 3. (a) GVD and (b) the nonlinear parameter for the NL-15-670 fiber from Crystal Fibre, using an assumed value of  $n_2 = 1.81 \times 10^{-20} \text{ m}^2/\text{W}$  [22] for a range of fiber diameters. Also shown is (c) the pulse width and (d) a representation of the SSFS rate, calculated with Eqs. (15) and (7), respectively, for an initial soliton of energy  $E_0 = 100 \text{ pJ}$  at  $\lambda_0 = 2\pi c/\omega_0 = 850 \text{ nm}$ . In each panel results are shown for three ratios of the tapered to the untapered fiber diameter: 1.0 (solid curves), 0.8 (dashed) and 0.6 (dotted-dashed). The dotted vertical lines indicate the long-wavelength edge of the anomalous dispersion region for the three diameter scalings.

linearity, leading to an increase in the shift rate toward longer wavelengths. This effect may be clearly observed for the scaling ratios of 1.0 and 0.8 in Fig. 3(d). The spectral width of the soliton and the level of higher-order dispersion will ultimately determine to what degree this enhancement can be realized in a more accurate pulse propagation model.

The enhancement of the shift rate due to the reduced core diameter is accompanied by a reduction in the extent of the region of anomalous dispersion, as well as a shortening of the ZDWs. Not only are the bright soliton solutions employed above based on the assumption of anomalous dispersion, but a soliton impinging on a point of zero dispersion sheds energy in the form of resonant, normally DWs, and the redshift of the soliton is halted by the resultant spectral recoil [10]. The enhancement of the SSFS in a uniform waist taper is therefore limited if the scaling of the waist is such that the soliton reaches the second ZDW before the end of the taper. There then exists the possibility of varying the waist diameter along the length of the taper such that, as the soliton approaches the longer of the ZDWs due to the SSFS, the region of anomalous dispersion is extended to allow the pulse to continue to redshift. In this way, a modest enhancement of the SSFS rate over that in an untapered fiber can be achieved while avoiding the limitation to the redshift arising in a taper with a constant waist diameter (cf. Fig. 1).

### 3. NUMERICAL MODELING

#### A. General Method

We have simulated pulse propagation in a number of scenarios by numerically solving Eq. (1) using the split-step

Fourier method [6] with a local error threshold of  $10^{-5}$  [21]. The simulations were carried out on a frequency domain spanning  $\sim 900$  THz, centred on  $\lambda_0 = 850$  nm discretized into  $2^{17}$  bins. This implies a temporal window of width  $\sim 150$  ps. We include higher-order dispersion terms up to  $\beta_{15}$  and retain up to  $\gamma_2$  in the expansion of the nonlinear coefficient. For the material parameters of bulk silica we use  $n_2 = 1.81 \times 10^{-20}$  m<sup>2</sup>/W [22] and  $f_R = 0.18$  [23]. In each case an initial pulse corresponding to an ideal fundamental soliton of specified initial energy  $E_0$  centered at  $\lambda_0$  was propagated over 1 m of the fiber described in Fig. 3 for a particular diameter profile. The merit of a specific taper profile is taken to lie in the wavelength  $\lambda_s$  of the soliton attained at the end of the fiber, along with the ratio of the final pulse energy lying in the anomalous dispersion region  $E_a$  to the total final energy  $E_f$  (i.e., including any resonantly emitted DWs);  $\lambda_s$  is taken to be the location of the peak in this truncated spectral region.

In order to concentrate on the propagation effects in the taper waist we launch a soliton directly into this part of the fiber; that is, we do not consider pulse propagation in the transition regions connecting the taper waist to the untapered fiber. The soliton is assumed to adapt adiabatically to the transition in fiber parameters, which has been confirmed numerically for a transition length of a few centimeters, and the variation of the contribution to the total redshift in these regions for different waist scalings is ignored.

We also compare the dynamics of the full theory, embodied in Eq. (1), with the redshift predicted by Eq. (7). The simplified theory described in Section 2 is expected to perform well where the emission of DWs is avoided and the ideal soliton solution remains an accurate approximation to the true form of the pulse. Solution of the idealised problem is significantly less numerically intensive than implementing the full generalized NSE, and so can provide a more convenient method for studying the SSFS in tapered fibers.

### B. Tapers with an Axially Uniform Waist

In Fig. 4 we show results from several full simulations [i.e., solving Eq. (1)] of a soliton with  $E_0 = 100$  pJ propagating in a uniform taper waist for various diameter scal-

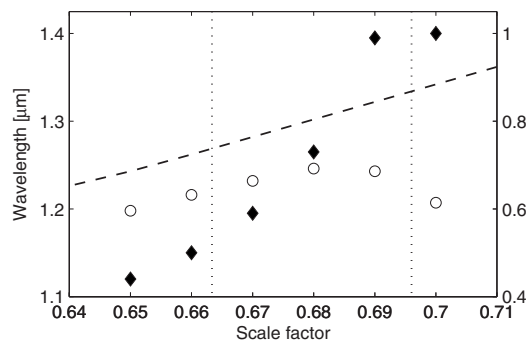


Fig. 4. Left axes, final  $\lambda_s$  (circles) and the second ZDW in the waist (dashed line). Right axes,  $E_a/E_f$  (diamonds). The data shown relate to the propagation of an initial soliton with  $E_0 = 100$  pJ along a 1 m taper waist for various uniform diameter scalings, simulated by using Eq. (1). The simulations corresponding to the data points lying between the vertical dotted lines are depicted in more detail in Fig. 5.

ings. The final wavelength achieved by the soliton is observed to increase with the decreasing core size until the proximity of the soliton to the second ZDW before the end of the taper waist is such that significant emission of DWs occurs. This latter process is indicated by the fall in the fraction of the total final pulse energy lying in the anomalous dispersion region at the end of the waist. The redshift of the soliton is thus reduced because of a reduction in its energy and the effect of the spectral recoil. As the second ZDW is reduced and the redshift rate increased by further reduction in the waist diameter, the final wavelength of the soliton is limited to values below those achievable in tapers of lower nonlinearity, with a respective increase in losses to DWs due to the soliton spending a larger fraction of the taper length impinging upon the normal dispersion region. Thus, for the initial soliton and the waist length used here, there is an optimal waist scaling  $\sim 0.68$  at which the SSFS is maximized. The curve traced out by the points in Fig. 5 corresponding to the final soliton wavelengths is relatively flat around the optimal scaling point. From an experimental point of view, obtaining this optimum may thus be somewhat difficult, although it may also be viewed as an advantage in that small errors in the actual scaling factor are not expected to have a significant effect on the maximum wavelength achievable. We do, however, note the marked changes in the final fraction of the total energy in the anomalous dispersion region across this range of diameter scalings where the final soliton wavelength does not change appreciably. In any case, the most important fact is clear; namely, that a continued reduction of the waist diameter below the optimal scaling leads to a reduction in the final wavelength and energy associated with the soliton.

The spectral evolution of the pulses corresponding to the data points lying between the vertical dotted lines in Fig. 4 are illustrated in Fig. 5, along with the dynamics in the untapered fiber. The enhancement of the SSFS in the tapered fibers over that in the untapered case can be clearly seen, along with the resonant growth of DWs in the tapers with the two lowest diameter ratios. It may

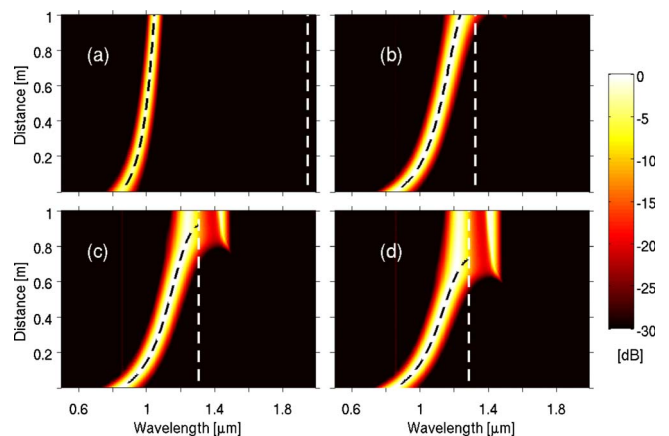


Fig. 5. (Color online) Spectral evolution of an initial ideal fundamental soliton with  $E_0 = 100$  pJ for three uniform scalings of the fiber waist diameter relative to the untapered fiber: (a) 1.00, (b) 0.69, (c) 0.68, and (d) 0.67. The white dashed lines indicate the position of the second ZDW in each case, while the black dashed curves show the evolution of the soliton center frequency predicted by Eq. (7).

also be observed that, near the point of optimal scaling, it requires only a small fractional change in the waist diameter ( $\sim 0.01\%$ ), and consequently in the ZDW, to provoke a marked variation in the spectral evolution.

Also shown in Fig. 5 is the evolution of the soliton center wavelength as predicted by Eq. (7). As expected, the simplified theory performs well for scalings of 1.00 and 0.69, where the emission of DWs is negligible, but incorrectly predicts the attainment and traversal of the ZDW by the soliton in the remaining two cases where DW emission is strong and the soliton redshift is subsequently cancelled at a wavelength below this point. Furthermore, the dispersion-enhanced shift rate predicted by the simplified theory on approach to the ZDW for the scalings of 0.67 and 0.68 is not borne out in the full simulations because of the spectral width of the soliton being such that the redshift cancellation by DW emission halts the SSFS before this enhancement may take effect.

### C. Tapers with an Axially Nonuniform Waist

The purpose of the tapers with a varying waist diameter proposed here is to provide the maximum nonlinearity possible at the instantaneous soliton center frequency while avoiding the emission of DWs. Since the amplitude of the DWs emitted is proportional to the spectral amplitude of the soliton at the radiation frequency [24], one could, from a design point of view, aim to keep this quantity at or below some threshold value along the length of the taper; this is the approach we pursue here. The spectral amplitude at the resonant frequency for DWs translates to a dimensionless spectral shift  $\Delta\Omega = \Delta\omega T_s$ , where  $\Delta\omega$  is the difference between the soliton center frequency and the resonant frequency. To lowest order we have  $\Delta\omega = 3|\beta_2|/|\beta_3|$ , and, from Eq. (15), our threshold condition becomes

$$\frac{6|\beta_2(\bar{\omega})|^2}{\gamma(\bar{\omega})E(\bar{\omega})|\beta_3(\bar{\omega})} \geq \Delta\Omega_{\min}, \quad (20)$$

where  $\Delta\Omega_{\min}$  represents the minimum spectral offset. Since the left-hand side of the expression above is expected to be most sensitive to the GVD near the ZDWs, we approximate the condition expressed in Eq. (20) by requiring that

$$|\beta_2(\bar{\omega})| \geq |\beta_2|_{\min}, \quad (21)$$

where  $|\beta_2|_{\min}$  is the minimum GVD tolerated at  $\bar{\omega}$ . We find the implementation of this last condition to be sufficient for our purposes. Thus, we design a taper with a longitudinally varying waist diameter by requiring that the soliton, once it has entered the waist region, maintains a level of GVD at its central frequency that is at or below a threshold value. In this sense, the taper profile is designed dynamically as the soliton propagates.

The spectral dynamics of an initial ideal soliton for which  $E_0 = 100$  pJ are shown in Figs. 6(a)–6(c) for three optimized, axially nonuniform tapers with different GVD threshold values. After a short initial uniform length of waist the soliton reaches the threshold GVD, and the waist begins to widen, as indicated by the increasing ZDW. Since the rate at which the second ZDW increases, and therefore the rate of uptapering, is directly linked to

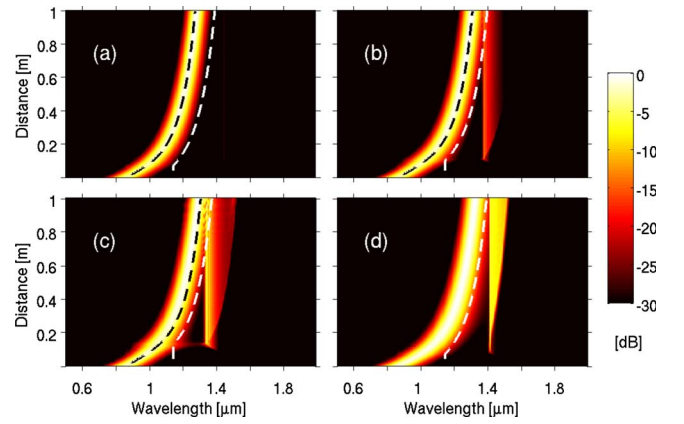


Fig. 6. (Color online) Spectral evolution of an initial ideal fundamental soliton with  $E_0 = 100$  pJ for tapers with axially nonuniform waists designed with a minimum waist scaling of 0.60 and a GVD threshold of (a)  $-70$ , (b)  $-60$ , and (c)  $-50$  ps<sup>2</sup>/km. Also shown (d) is the spectral evolution of a soliton with  $E_0 = 110$  pJ propagating in the taper from (a). The white dashed curves indicate the position of the second ZDW in each case, while in (a)–(c) the black dashed curve shows the evolution of the soliton center frequency predicted by Eq. (7).

the rate of redshift of the soliton, the rate of widening of the waist slows with propagation distance as the soliton moves to spectral regions of lower nonlinearity and loses energy owing to the inelastic scattering process.

In comparing the pulse propagation for the three GVD thresholds of  $-50$ ,  $-60$ , and  $-70$  ps<sup>2</sup>/km, the most notable difference is the level of DW emission. For the highest absolute threshold value of  $|\beta_2|_{\min} = 70$  ps<sup>2</sup>/km there is no observable emission of DWs on the scale displayed in Fig. 6, and the soliton attains a final peak wavelength of  $\lambda_s = 1.283$   $\mu\text{m}$  with a ZDW at the termination of the waist region of  $\lambda_{\text{ZD}} = 1.387$   $\mu\text{m}$ . Reduction of the threshold to  $|\beta_2|_{\min} = 60$  ps<sup>2</sup>/km leads to the generation of a small DW feature (of peak value  $< -10$  dB), an increased final soliton wavelength of  $\lambda_s = 1.306$   $\mu\text{m}$ , and a final ZDW of  $\lambda_{\text{ZD}} = 1.392$   $\mu\text{m}$ . The increased redshift follows from the soliton's experiencing a higher shift rate due to a closer proximity to the second ZDW [cf. Fig. 3(d)]. Further reduction of the threshold to  $|\beta_2|_{\min} = 50$  ps<sup>2</sup>/km sees significant generation of low-amplitude DWs due to the increased overlap of the soliton spectrum with the resonant normal dispersion region. Thus, despite the lower dispersion experienced by the soliton contributing to an increase in the energy density as a result of temporal pulse compression, the energy transfer from the soliton to DWs reduces the shift rate, and the soliton achieves a lower final wavelength of  $\lambda_s = 1.295$   $\mu\text{m}$ . We also note that discussion of the relative fractions of the final pulse energy in the normal and anomalous dispersion regions does not necessarily lead to a good indication of the merit of a taper in the axially nonuniform case, since much of the energy initially emitted as normally DWs can lie in the anomalous dispersion regime at the end of the waist as in Figs. 6(b) and 6(c).

As a testament to the enhancement of the SSFS rate in the optimized, axially nonuniform tapers over those with a uniform waist, the maximum wavelength achieved in

the simulations shown herewithin is 60 nm higher in the nonuniform geometry. In comparing simulations where the resonant emission of DWs is negligible, the nonuniform tapers possess a higher average nonlinearity than their uniform counterparts. It is this property, in a slightly simplified reasoning, that leads to the relative enhancement of the SSFS. This simplification is possible because, for the basic fiber and initial pulse parameters chosen here, the bandwidth of the solitons is such that the dispersion-induced enhancement of the SSFS rate in the vicinity of the second ZDW cannot be effectively exploited while simultaneously avoiding strong conversion of pulse energy into low-amplitude DWs. Thus, the general enhancement of the redshift observed in the optimized tapers is relatively modest. This could be improved with a choice of parameters that lead to a soliton spectrum narrow enough to exploit the dispersion-enhanced shift seen in Fig. 3(d).

The taper profiles presented in Figs. 6(a)–6(c) have been designed for a soliton of a specific initial energy, namely, 100 pJ. Increasing the initial pulse energy in the taper from the first example to 110 pJ [cf. Fig. 6(d)] leads to 22% of the final pulse energy lying in the normally dispersive regime at the end of the taper, while the final wavelength of the soliton is 42 nm above that reached by the optimal pulse for which the taper was designed. Initially, the higher pulse energy leads to an increased redshift over the lower-energy pulse. Then, as the soliton encounters the ZDW at the beginning of the waist, it experiences a loss of energy to DWs along with an accompanying spectral recoil until its energy is matched to the taper profile and it continues to redshift. In this way the resonant emission of low-amplitude radiation is used as a method by which the soliton, for which the taper design is not ideal, may adapt itself to match the longitudinally varying dispersion and nonlinearity in the taper waist. A consequence of this process is a robustness of the longitudinally variable taper design to an input soliton of energy higher than the ideal value, in that the final wavelength achieved is not compromised. Of course, if the input energy of the soliton is lower than the ideal value, the final wavelength is reduced as in a standard taper, or untapered fiber; indeed, it is this behavior that leads to the tunability of the output wavelength. In the same vein, an increase of the initial wavelength of the soliton by 10 nm in the same taper leads to a final wavelength of  $\lambda_s = 1.326 \mu\text{m}$ , while a reduction of  $\lambda_0$  by the same amount results in  $\lambda_s = 1.244 \mu\text{m}$ . Thus, one must ensure that the input wavelength of the soliton is at or above the design wavelength of the taper in order to obtain any advantage from the nonuniform geometry.

A comparison of the full simulations with the simplified theory is made in Figs. 6(a)–6(c), where the taper profiles are determined as the pulse propagates. The evolution of the soliton center frequency predicted by Eq. (7) is a marginal underestimation in the example of Fig. 6(a), while in Fig. 6(b) the small reduction of the soliton energy due to the DW emission helps to compensate for this error. Finally, in the example of Fig. 6(c), a larger transference of energy from the soliton in the more complete model leads to the idealized theory predicting a slightly higher redshift. Nonetheless, for simulations where the interaction

of the soliton with DWs is weak, the predictions of the SSFS following from the assumption of an ideal fundamental soliton adapting adiabatically to the local environment are generally within 1% of the results arising from the solution of Eq. (1), even when the simulations involve a taper with an axially varying waist diameter.

#### 4. DISCUSSION AND CONCLUSION

The increase of the nonlinearity resulting from the reduced core size in a uniformly tapered optical fiber generally leads to an enhancement of the SSFS. However, if an arbitrary scaling down of the waist diameter leads to the soliton reaching the long-wavelength edge of the anomalous dispersion region before the end of the taper, the SSFS can be limited below that achievable with a larger core size.

We have shown in principle that a longitudinal variation in the waist diameter of a photonic crystal fiber taper can be designed in such a way that the SSFS is enhanced over that possible in a taper with a uniform waist, although the enhancement in the wavelength shift is only of the order  $\sim 5\%$ . Of course, any particular taper as designed here is optimized for a soliton with a specific energy and initial frequency. This does not affect the tunability of the final wavelength, however, which may be achieved as in standard geometries by reducing the initial pulse energy. An increase in the initial energy leads to a higher shift rate than that for which the taper was designed, and thus to impingement of the soliton upon the second ZDW. Despite the resultant resonant emission, however, the pulse continues to redshift as the ZDW moves to longer wavelengths and the soliton self-regulates its energy through continued radiation. The enhanced redshift is also seen to be robust with regard to small increases to the input wavelength where a similar regulation process occurs.

In an actual taper the waist diameter profile, and therefore the longitudinal variation of the second ZDW, is a fixed property of the fiber to which the soliton responds as it propagates. In the simulations of the longitudinally varying tapers performed here, however, the taper profile is designed during propagation as a response to the spectral motion of the soliton along with the dispersion threshold requirement. Actual realization of such a taper would be difficult, since, in order that it be effective, the input energy and wavelength of the soliton must be well matched to the design parameters. Furthermore, the performance of the taper is expected to be sensitive to effects such as scattering losses and geometric nonideality arising in the fabrication process. However, these complications may be mitigated if the wavelength and energy of the initial soliton is higher than the ideal values corresponding to the taper design. Finally, the principles demonstrated here make clear some of the subtleties relating to soliton propagation in tapered optical fibers; specifically, the existence of an optimal scaling for uniform waist tapers and, in principle, the possibility of dispersion-enhanced SSFS in the vicinity of the second ZDW.

## REFERENCES

1. F. M. Mitschke and L. F. Mollenauer, "Discovery of the soliton self-frequency shift," *Opt. Lett.* **11**, 659–661 (1986).
2. N. Nishizawa and T. Goto, "Compact system of wavelength-tunable femtosecond soliton pulse generation using optical fibers," *IEEE Photon. Technol. Lett.* **11**, 325–327 (1999).
3. M. E. Fermann, A. Galvanauskas, M. L. Stock, K. K. Wong, D. Harter, and L. Goldberg, "Ultrawide tunable Er soliton fiber laser amplified in Yb-doped fiber," *Opt. Lett.* **24**, 1428–1430 (1999).
4. J. H. Lee, J. van Howe, C. Xu, and X. Liu, "Soliton self-frequency shift: experimental demonstrations and applications," *IEEE J. Sel. Top. Quantum Electron.* **14**, 713–723 (2008).
5. S. Leon-Saval, T. Birks, W. Wadsworth, P. S. J. Russell, and M. Mason, "Supercontinuum generation in submicron fibre waveguides," *Opt. Express* **12**, 2864–2869 (2004).
6. G. P. Agrawal, *Nonlinear Fiber Optics* (Academic, 2007).
7. X. Liu, C. Xu, W. H. Knox, J. K. Chandalia, B. J. Eggleton, S. G. Kosinski, and R. S. Windeler, "Soliton self-frequency shift in a short tapered air-silica microstructure fiber," *Opt. Lett.* **26**, 358–360 (2001).
8. S. M. Kobtsev, S. V. Kukarin, N. V. Fateev, and S. V. Smirnov, "Generation of self-frequency-shifted solitons in tapered fibers in the presence of femtosecond pumping," *Laser Phys.* **14**, 748–751 (2004).
9. D. V. Skryabin, F. Luan, J. C. Knight, and P. S. J. Russell, "Soliton self-frequency shift cancellation in photonic crystal fibers," *Science* **301**, 1705–1708 (2003).
10. F. Biancalana, D. V. Skryabin, and A. V. Yulin, "Theory of the soliton self-frequency shift compensation by the resonant radiation in photonic crystal fibers," *Phys. Rev. E* **70**, 016615 (2004).
11. B.-W. Liu, M.-L. Hu, X.-H. Fang, Y.-F. Li, L. Chai, C.-Y. Wang, W. Tong, J. Luo, A. A. Voronin, and A. M. Zheltikov, "Stabilized soliton self-frequency shift and 0.1-pHz sideband generation in a photonic-crystal fiber with an air-hole-modified core," *Opt. Express* **16**, 14987–14996 (2008).
12. J. C. Travers and J. R. Taylor, "Soliton trapping of dispersive waves in tapered optical fibers," *Opt. Lett.* **34**, 115–117 (2009).
13. Z. Chen, A. J. Taylor, and A. Efimov, "Coherent mid-infrared broadband continuum generation in non-uniform ZBLAN fiber taper," *Opt. Express* **17**, 5852–5860 (2009).
14. J. M. Dudley, G. Genty, and S. Coen, "Supercontinuum generation in photonic crystal fiber," *Rev. Mod. Phys.* **78**, 1135 (2006).
15. K. J. Blow and D. Wood, "Theoretical description of transient stimulated Raman scattering in optical fibers," *IEEE J. Quantum Electron.* **25**, 2665–2673 (1989).
16. J. P. Gordon, "Theory of the soliton self-frequency shift," *Opt. Lett.* **11**, 662–664 (1986).
17. R. H. Stolen, E. P. Ippen, and A. R. Tynes, "Raman oscillation in glass optical waveguide," *Appl. Phys. Lett.* **20**, 62–64 (1972).
18. J. Herrmann and A. Nazarkin, "Soliton self-frequency shift for pulses with a duration less than the period of molecular oscillations," *Opt. Lett.* **19**, 2065–2067 (1994).
19. A. A. Voronin and A. M. Zheltikov, "Soliton self-frequency shift decelerated by self-steepening," *Opt. Lett.* **33**, 1723–1725 (2008).
20. Document NL-15-670.pdf may be obtained at <http://www.nktphotonics.com/side5328.html>.
21. O. Sinkin, R. Holzlohner, J. Zweck, and C. R. Menyuk, "Optimization of the split-step Fourier method in modeling optical-fiber communications systems," *J. Lightwave Technol.* **21**, 61–68 (2003).
22. F. A. Oguama, H. Garcia, and A. M. Johnson, "Simultaneous measurement of the Raman gain coefficient and the nonlinear refractive index of optical fibers: theory and experiment," *J. Opt. Soc. Am. B* **22**, 426–436 (2005).
23. R. Hellwarth, J. Cherlow, and T.-T. Yang, "Origin and frequency dependence of nonlinear optical susceptibilities of glasses," *Phys. Rev. B* **11**, 964–967 (1975).
24. N. Akhmediev and M. Karlsson, "Cherenkov radiation emitted by solitons in optical fibers," *Phys. Rev. A* **51**, 2602–2607 (1995).